

Azimuth ambiguity removal and non-linear force-free extrapolation of near-limb magnetic regions

Solar Physics

G. V. Rudenko¹ · I. I. Myshyakov¹ · S. A. Anfinogentov¹ ·

© Springer ●●●●

Abstract Possibilities in principle for satisfactory removal of the 180°-azimuthal ambiguity in the transverse field of vector magnetograms and the extrapolation of magnetic fields independently of their position on the solar disk are shown. Revealed here is an exact correspondence between the estimated field and the nonpotential loop structure on the limb.

The Metropolis's algorithm modified to work in spherical geometry is used to resolve the azimuthal ambiguity. Based on a version of the optimization method from Rudenko and Myshyakov (2009), we use corrected magnetograms as boundary conditions for magnetic field extrapolation in the nonlinear force-free approximation.

Keywords: Magnetic fields, Corona; Force-free fields; azimuthal ambiguity

1. Introduction

Removing azimuth ambiguities is a necessary condition for using vector magnetograms to detect a real magnetic structures and understand the nature of active solar regions. At present we have many methods and approaches providing a successful solution to this problem but only for regions nearby the disk center or at a medium distance from it (Metcalf (1994); Moon *et al.* (2003); Cuperman and Semel (1993) Georgoulis *et al.* (2004); Georgoulis (2005); Gary and D'emoulin (1995); Canfield *et al.* (1993); Leka and Skumanich (1999); Pevtsov *et al.* (1995);). For this reason near-limb regions are not available for effective use. Thus a considerable part of collected and constantly reproduced valuable solar data, most searched in various investigations related to region physics and prediction of their activity, is lost. The key problem of many methods for resolving azimuth ambiguities (including the minimum energy method applied in this work) is to construct correctly a near-boundary model of potential or linear force-free fields answering strictly to the longitudinal component of a photospheric field being measured. The solution to this problem is

¹ Institute of Solar-Terrestrial Physics SB RAS, Lermontov St. 126, Irkutsk 664033, Russia email: rud@iszf.irk.ru email: ivan_m@iszf.irk.ru email: anfinogentov@iszf.irk.ru

quite simple and successful only for central regions. Both getting a near-boundary model of potential or linear force-free field and the rest of the technique for removing azimuth ambiguities are to level most of the negative influence associated with necessary flat approximation of the spherical part of a region. For a number of reasons, this negative influence is most pronounced in distal regions. In this regard, any examples of successful removing of a near-limb vector magnetogram azimuth ambiguity and subsequent reproduction of a real near-limb 3D structure from a prepared complete boundary vector field are of fundamental importance.

In this paper, we propose a method for solving the azimuth ambiguity problem for near-limb regions and test it on model and real data. In case of model data, correctness of the azimuth ambiguity removal can be easily verified. Otherwise, in case of real data it can be estimated only indirectly. We make such estimation by performing NLFF extrapolation, relying on corrected vector magnetogram, and comparing extrapolated field lines to real loop structures. For NLFF extrapolation we use the optimization method Gary and D'emoulin (1995) as implemented in Rudenko and Myshyakov (2009) (FOM). Using this version, the authors of Rudenko and Myshyakov (2009) managed to reproduce a non-potential sigma field structure observed at a medium distance from the center. Clearly, the correctness of real field extrapolation depends first of all on the correctness of boundary transverse field disambiguation. On the other hand, the evidence of successful solution to the problem of ambiguity may be a correspondence between the extrapolated field and observed coronal features. Actually, we use the studied example to conduct an interrelated test of two techniques aimed at solving various problems: azimuth ambiguity removal and NLFF extrapolation as applied to near-limb regions.

FOM of NLFF extrapolation is described in detail in Rudenko and Myshyakov (2009). Here it is applied in its original form, without modifications. The method for removing azimuth ambiguity rests on the minimum energy method (Metcalf, 1994). This paper presents the following components of this method:

- translation of data in the form of artificial Stokes parameters into the working "quasi-spherical" coordinate system (Rudenko and Myshyakov, 2009) succeeded by smoothing to reduce noise component of the transverse field and with the inverse transformation to the vector form;
- FFT extrapolation of the boundary potential field with constant direction of the oblique derivative corresponding to the observed line-of-sight component in the "quasi-spherical" coordinate system;
- modification of the minimum energy method to spherical geometry with no need for data grid uniformity ("spherical" minimum energy method).

2. Preliminary transformations of initial data

2.1. Transformation of initial vector magnetogram data into artificial Stokes parameters

A data set specified on the uniform grid of rectangle of the picture plane will be taken as an initial magnetogram: B_x is the line-of-sight magnetic field component; B_y and B_z are transverse field components with the 180° ambiguous azimuth φ . Let us define the transformation of initial data into new variables of artificial Stokes parameters:

$$\begin{aligned}
V &= B_x, & Q &= B_{\perp} \cos(2\varphi), & U &= B_{\perp} \sin(2\varphi), \\
B_{\perp} &= \sqrt{B_y^2 + B_z^2}, & \varphi &= \arctan(B_z/B_y).
\end{aligned}
\tag{1}$$

All V, Q, U values are unambiguous. Using Equation (1), we can always return to field variables which not necessarily coincide with initial transverse components. We can apply interpolation and smoothing operations to artificial Stokes parameters (in contrast to the indefinitely directed transverse field) without loss of physical connections between transverse field components. For instance, we can interpolate data without quality loss into another grid, including nonuniform one, smooth them and then return to the field form.

2.2. Transformation of data into a coordinate system of the quasi-spherical space

Azimuth disambiguation method and the NLFF extrapolation require transforming data into a uniform grid of the lower plane of the square box in the quasi-spherical space. The coordinate system of the quasi-spherical space working area relies on the auxiliary coordinate system where a conditionally chosen center of magnetogram is at the solar disk center $[R_{Sun}, 0, 0]$. Longitude and latitude in radians define horizontal coordinates in the quasi-spherical space. This coordinate system is thoroughly described in Rudenko and Myshyakov (2009). Next we consider the introduced coordinate system as Cartesian in which the model field divergence is zero and the strict condition of force-free approximation is valid. A desired boundary field is specified as follows:

- a uniform grid is plotted on a quasi-spherical surface with a spatial resolution scale less than the minimum scale of the data grid spatial resolution;
- initial magnetogram parameters V, Q and U of Equation (1) are interpolated into nodes of the uniform grid of the working space lower plane and, if necessary, the obtained data are smoothed and interpolated into the desired uniform grid;
- data are transformed into the normal vector form;
- vector transformations of the field into the quasi-spherical coordinate system are possible only after the azimuth ambiguity problem is solved.

3. Potential field calculations

After having transferred data to the working boundary plane, we can use only a line-of-sight field component (B_x - in the initial coordinate system). To compute the potential field, we obtain representation of the line-of-sight unit vector corresponding to the magnetogram center in the working coordinate system. Next, in FFT format we solve the trivial boundary Laplace problem with the oblique derivative of constant direction. We use the potential field in the spherical minimum energy method and to construct an initial field in the 3D box for FOM.

Note that a similar geometric scheme can be easily applied to solve the boundary problem of the force-free extrapolation with a given constant α

4. Modification of the minimum energy method (spherical minimum energy method)

The minimum energy method Metcalf (1994) implements the problem of searching a state corresponding to the global minimum of the positively defined additive function of $\nabla \cdot \mathbf{B}$ and J_n simulating energy characteristic of the statistical system. The problem-solving method rests on the well-known and widely used method simulating the annealing process (Metcalf *et al.* (2006); Kirkpatrick *et al.* (1993); Metropolis *et al.* (1953)) and, as applied to the azimuth ambiguity problem, is discussed in detail in Metcalf (1994). Our modification of this method Metcalf (1994) concerns only changes in the technique of determining local values $\nabla \cdot \mathbf{B}$ and J_n and configuration of an elementary micro-ensemble specifying "temperature" characteristic. This modification simplifies the technique of determining $\nabla \cdot \mathbf{B}$ and J_n on the sphere and can work equally well on arbitrary nonuniform grids, including the one that corresponds to uniform distribution of node projections onto picture plane.

To construct the local "Energy" function, we apply Gaussian and Stokes integral theorems to the elementary, arbitrary spherical triangle whose vertices and edges correspond respectively to three nearest nodes of the chosen grid and to geodetic intervals jointing vertices. In this method, desired $\nabla \cdot \mathbf{B}$ and J_n values may be expressed in the form independent of the chosen coordinate system.

$$\begin{aligned} \nabla \cdot \mathbf{B} &\approx \frac{1}{2Sh} \left[\sum_i (\overline{\mathbf{B}}_i^{dat} \cdot \mathbf{n}_i) 2hl_i + \sum_j (\overline{\mathbf{B}}_j^{pot} \cdot \mathbf{n}_j) s_j \right] \approx \\ &\approx \frac{1}{S} \sum_i (\overline{\mathbf{B}}_i^{dat} - \overline{\mathbf{B}}_i^{pot}) \cdot \mathbf{n}_i l_i \end{aligned} \quad (2)$$

$$j_n \approx \frac{1}{S} \sum_k \overline{(B \cdot \tau)}_k l_k \quad (3)$$

Here S is the spherical triangle area; h is the spherical prism half-height intersected in the middle by the sphere surface; l is length geodesic connecting the vertices of the spherical triangle; index i corresponds to the chosen numbering of lateral faces; j denotes upper and lower faces; \mathbf{n}_i and \mathbf{n}_j are unit vectors of outer normals of lateral and upper-lower faces respectively; s_j are spherical triangle areas of upper-lower faces; dashes over field vectors in Equation (2) correspond to the mean vector of field from two vertices in the plane corresponding to the lateral surface; index k in Equation (3) numbers consecutively spherical triangle edges; the dash over the bracket in Equation (3) denotes the average of two scalar product fields at vertices of the edge by boundary unit vectors τ tangent to the geodetic line, jointing corresponding pair of vertices directionally ordered in accordance with the general direction of rotation by the corkscrew rule. To better understand Equations (2) and (3), we give (Figure 1) a discrete representation of integrals through a lateral face of the spherical prism and through an edge of the spherical triangle in vertices of which the full vector of the magnetic field under measure is specified.

To construct the divergence of \mathbf{B} , we replace the unknown field on the upper and lower faces of the spherical prism by the potential field and then use the strict

$$\int_{(A'A''B''B')} \mathbf{B} \cdot \mathbf{n}_i ds \rightarrow (\overline{\mathbf{B}_i \cdot \mathbf{n}_i}) 2hl_i; \quad \overline{\mathbf{B}_i} = (\mathbf{B}_A + \mathbf{B}_B) / 2$$

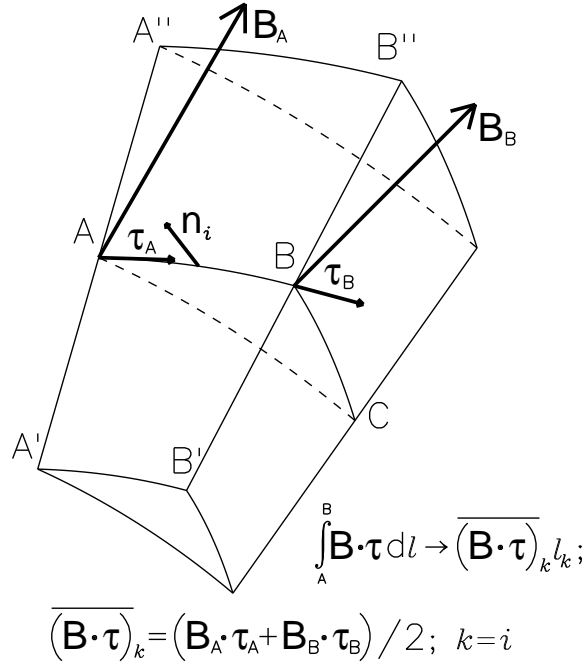


Figure 1. The illustration for Equations (2) and (3). Discrete approximations of integrals through a lateral face of the spherical prism and through an edge of the spherical triangle with vertices (A, B, C) on the photosphere.

equality to zero divergence of the potential field (a similar technique was applied in Metcalf (1994) to construct a divergence difference scheme).

As a result we use only nodal field values on the boundary surface to determine local "energy" ($E_{loc} = |\nabla \cdot \mathbf{B}| + |j_z|$) Elementary micro-ensemble "energy" corresponding to a chosen node is defined by the sum of local "energies" of all triangles for which the chosen node is one of their vertices.

We propose two release versions of the spherical azimuth ambiguity removal algorithm: a) on the quasisphere for subsequent extrapolation and b) on the magnetogram plane to correct only original magnetograms.

a) To each node of the quasispherical boundary surface corresponds a set of radius-vectors in the initial magnetogram coordinate system. We suppose that in nodes of the uniform quasi-spherical grid there are vector magnetic data transformed from original, ambiguous vector magnetograms in the manner of Section 2. We do not change here the coordinate representation of the vector field connected with

the magnetogram coordinate system. In the quasi-spherical coordinate system, we calculate a potential vector field (see Section 3) and express it in terms of coordinates of the initial coordinate system. Then we start the spherical azimuth ambiguity removal algorithm with input parameters (the field of radius-vectors, magnetic field of transformed data, and calculated potential field).

b) In the magnetogram coordinate system, we calculate radius-vectors corresponding to nodes of the uniform magnetogram grid. On the quasi-spherical grid at appropriate spatial resolution, we compute a potential field and interpolate it back into the magnetogram grid nodes with simultaneous transformation of its components into the magnetogram coordinate system. The obtained input data are used for the disambiguation. This version can be applied to direct disambiguation of magnetograms without changing positions of nodes on the magnetogram grid and thus without changing its original spatial resolution

In conclusion we would like to express our gratitude to the authors of the original version of the program "Minimum energy" for the free access to it on the web-site www.cora.nwra.com/AMBIG/. This alleviated the engineering problem of developing the program code for the modified version.

5. Testing with the analytical model of nonlinear force-free field

In the first test, we applied the spherical azimuth ambiguity removal and extrapolation algorithms to the limb magnetogram obtained from the analytical model of the nonlinear force-free field Low and Lou (1990). The model's parameters and geometrical layout were identical to those in Rudenko and Myshyakov (2009). The model magnetogram was calculated for the spherical surface near-limb part. At the entry, only the field component along the line of sight was considered unambiguous; the direction of the field transverse to the line of sight was considered ambiguous (180°). The test result is presented in Figures 2 and 3. In Figure 2, the upper pair of transverse components in the given model field is compared with the lower pair of transverse components after the azimuth disambiguation. Here we show the transverse field distribution on the quasi-spherical boundary surface where the azimuth ambiguity has been resolved. Figure 2 presents the correct removal of azimuth ambiguity throughout the magnetogram area. Only in two pixels, the direction of the transverse field of the disambiguated magnetogram forms an obtuse angle with the model's field direction. Here the position of the contours shows that the pixels are in the region of the transverse field's zero module where the algorithm can not be expected to determine an azimuth correctly. Figure 3 demonstrates effectiveness of the FOM algorithm for extrapolating the near-limb nonlinear force-free field. This follows from the correlation between green field lines of the model field and red ones of the calculated field.

6. Testings with real magnetograms

6.1. Exercises of near center

To test the spherical minimum energy method, we compare our disambiguated magnetograms with the ones (NOAA AR 10930) processed using the original version of

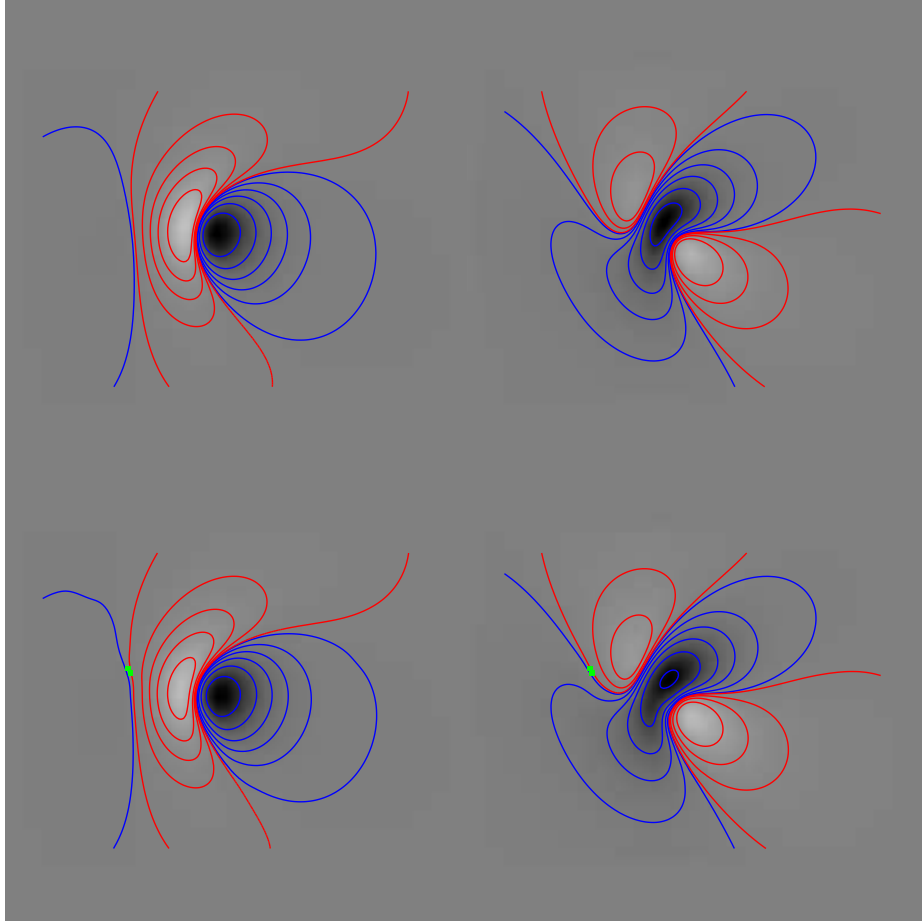


Figure 2. Transverse components of the magnetic field on the quasi-spherical boundary surface near the limb. On the top panel are field components of the nonlinear force-free dipole model (Low and Lou, 1990); on the lower panel are field components prepared for the extrapolation after the azimuth ambiguity had been resolved by the spherical minimum energy method. B_y (left), B_z (right). The contour lines correspond to a set of field magnitudes, red and blue lines are positive and negative values respectively. Pixels in which the angle between vectors of the transverse field in these magnetograms is over 90° are marked by green color.

minimum energy method in Schrijver *et al.* (2008)

(http://www.lmsal.com/~schryver/NLFFF/Hinode_SOT_SP_20061212_2030.fits) (Figure 4, *a*). The result of the processing of these magnetograms by the spherical minimum energy method is shown in Fig. 4 *b* and *c*: *b* - the disambiguation made on the quasi-spherical plane with smoothing over 7×7 nodes (version (*a*) in Section 4), resultant images are given in the plane of the sky of the magnetogram; *c* - the disambiguation made in the original nodes of the plane of the sky of the initial magnetogram (version (*b*) in Section 4). One can see that the structure elements of the transverse field \vec{b} and \vec{n} correspond, in the large, to the original magnetogram *a* except for the fragment denoted by an arrow. The marked fragment on the magnetogram *a* has a region with sharp boundaries that, in our opinion, indicates

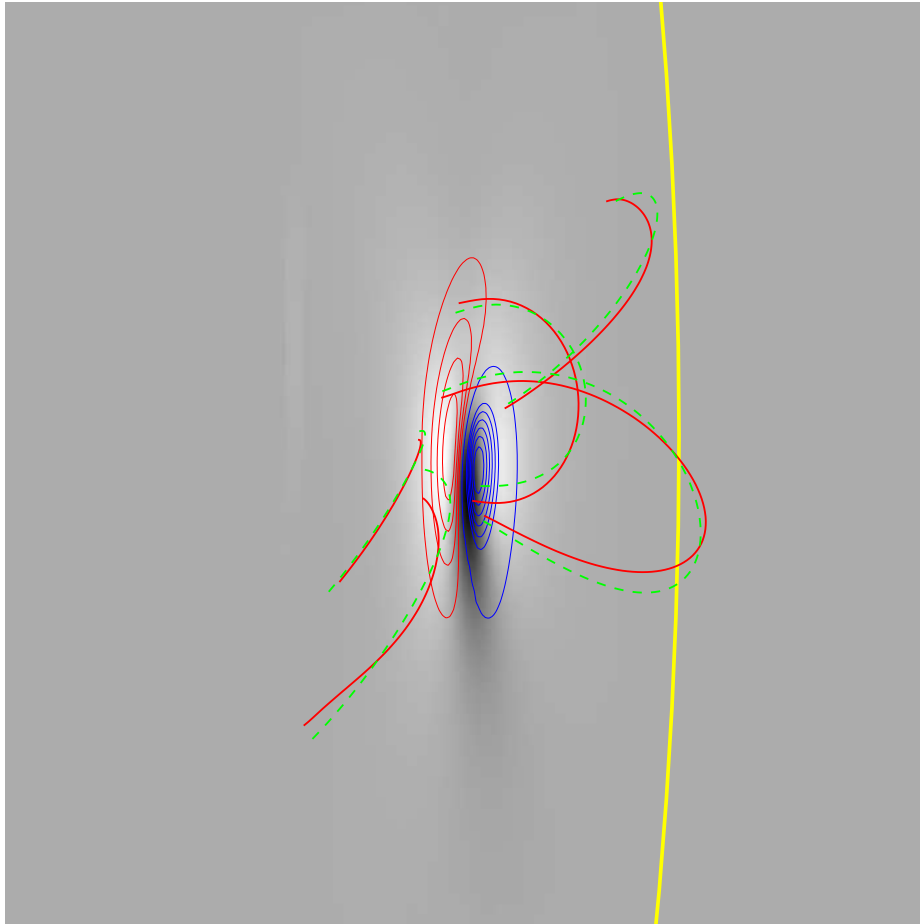


Figure 3. The comparison between calculated field lines (red) with those (green) of the model field in the plane of the sky of the solar disk ($[835.8'', 1006.2''] \times [-90.0'', 80.4'']$). The background is distribution of model field components along the line of sight; contour lines are distribution of the calculated normal field component; yellow line is the limb

misidentification of the azimuth. In our version (b, \tilde{n}), this part of the magnetogram looks more natural. Note that under close examination of the enlarged fragment of our magnetogram (c^*) at high spatial resolution one can see certain defects in the form of tortuous contrast channels. In fact, these defects are artificial and unrelated to algorithm errors in determining the azimuth. This is supported by the result of the processing we made at high resolution of the primary magnetogram SOT SP (Level 2) for 12 December 2006 20:30 UT. We have considered two variants of its preprocessing. In the first case, to comply with the spatial resolution of the magnetogram a , we carried out smoothing over 3×3 nodes and interpolation onto nodes of the magnetogram a using the technique of artificial Stokes parameters (in the manner of subsection 2.1). In the second case, we conducted direct smoothing and interpolation of the ambiguous transverse field components. The result of the first processing is shown in images d (d^*) of Figure 4. The defects discussed are

entirely absent here. In the second case (no images are given), the contrast channels manifested themselves in the same form. The data from the magnetogram must have been processed in the same manner. It is clear that any transformations of magnetograms in the ambiguous form break physical connections between original measurements and thus inevitably affect disambiguation results.

In closing this subsection let us point out the excellent agreement between results of the two geometric versions of spherical disambiguation (b , c) for the region near the disk center. Green color marks the regions in which the transverse field directions of over 100 Gauss in module differ in different magnetograms (these directions were compared on the quasi-spherical plane, where the high-resolution field (c) was presmoothed to bring it into line with smoothness of the field b).

6.2. Exercises of near the limb

To show the possibilities of correct determination of a transverse field direction and appropriate extrapolation of near-limb magnetic regions in the force-free approximation, we have chosen the vector magnetogram (SOT/SP level 2 "20061217_002528.fits") of the same magnetic region NOAA AR 10930 obtained at Space Observatory *Hinode*. The result of the complete cycle of its processing (disambiguation and extrapolation) is presented by the upper pair of the smoothed disambiguated magnetograms of the transverse field in Figure 5 and by the system of magnetic field lines of the calculated field which are superimposed on the image of loop structures in the X-ray image from *Hinode* XRT for 17 December 2006 0:24:20.5 UT (Figure 6, right). Due to real loop structures the force-free simulation model of the magnetic region seems to be much more preferable than the potential model (Figure 6, left). Figure 5 (bottom) shows that the result of the spherical disambiguation of the initial magnetogram in the plane of the sky at original spatial resolution (version (b) in Section 4) revealed that the azimuth in the region of the strong transverse field had been determined incorrectly. The reason for this might be related to fundamental limitations on work of the algorithm or to specific character of errors in near-limb measurements. The first reason may be excluded based on the secondary analysis we conducted using the artificial model of the full vector field of the real disambiguated photospheric magnetogram ¹. To construct this model, we used corrected components of the field of the magnetogram shown in Figure 4 (d). The model was made in the following manner: nodal values of the initial magnetogram field components were interpolated into nodes of the uniform grid (with unchanged scale of the initial spatial resolution) given in the Carrington spherical coordinate system invariant with respect to rotations; these field components were transformed into coordinate representation of the Carrington system. The invariant model simplified production of artificial magnetograms corresponding to a magnetic region position on the solar disk at a given time. Figure 7 demonstrates quality of the disambiguation of the artificial magnetogram corresponding to the exact position of the above real magnetogram. This figure shows close agreement between the two versions of spherical disambiguation and the initial artificial magnetogram and thus between each other. Defects in azimuth correction (color fractions) are in the region of the insignificant field

¹It is clear that the test made in Section 5 on the smooth analytical model does not adequately reproduce the complicated character of the real field distribution and gives insufficient grounds for efficiency of the algorithm

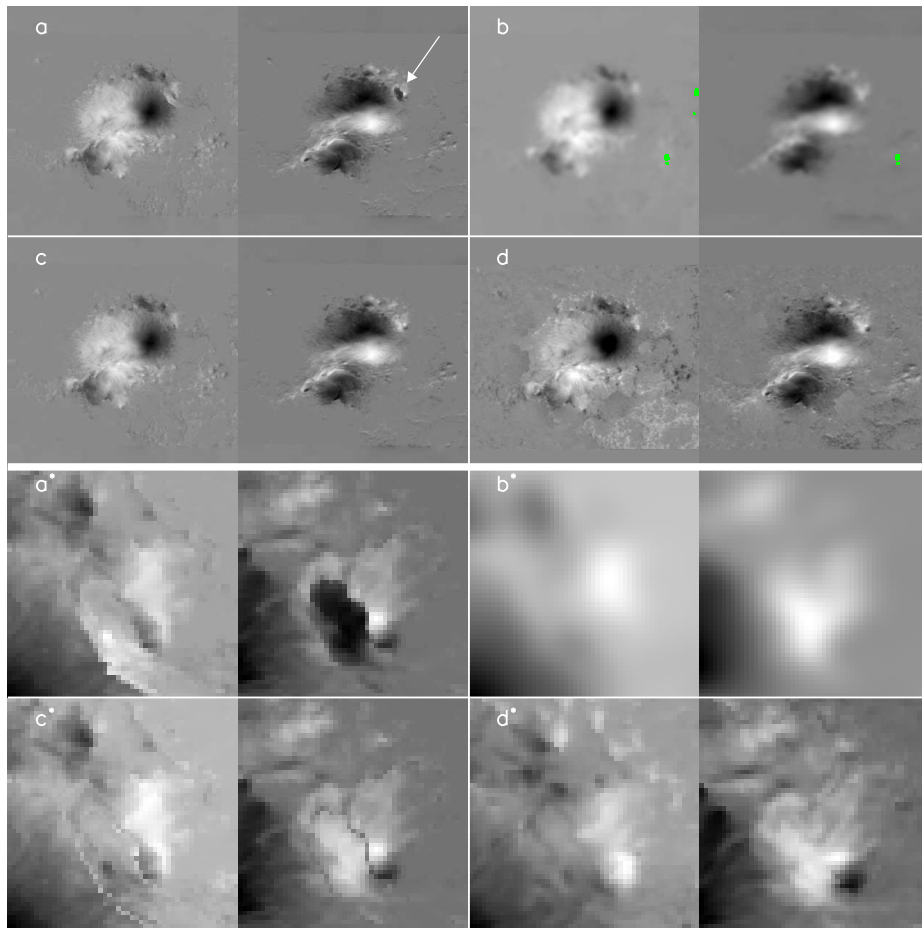


Figure 4. The transverse magnetograms of B_y, B_z : Hinode_SOT_SP_20061212_2030.fits (12 December 2006 20:30 UT) taken from <http://www.lmsal.com/schryver/NLFFF/> (a); the same magnetograms after the spherical disambiguation on the quasi-spherical plane with smoothing (b); the same magnetograms after the disambiguation (without smoothing) at high resolution on the grid uniform in the plane of the sky (c); original SOT SP (Level2) magnetograms (12 December 2006 20:30 UT) after the disambiguation (without smoothing) at high resolution on the grid uniform in the plane of the sky (d); a^*, b^*, c^* , and d^* are parts of corresponding magnetograms for the fragment of the plane-of-the-sky region indicated by an arrow. The green regions correspond to noncoincident directions of the transverse field > 100 Gauss on the quasi-spherical plane of the magnetogram c averaged on the quasi-spherical plane.

with relatively low amplitudes; i.e. quality of the spherical disambiguation can be recognized as adequate. Comparing these two versions of spherical disambiguation (in area of defects) shows a better quality of the version with smoothing. This probably reflects the efficiency of magnetogram noise suppression.

The last discussion raises a question of how far from the limb the correspondence between these two versions of spherical disambiguation remains valid. We can get a positive answer to this question by considering the nearest of the available magnetograms of this region measured 12 hours before the magnetogram under discussion

(Figure 8). In addition, the obtained transverse field configuration enables us to detect a small defect in correcting the azimuth of the top magnetogram in Figure 5 in the fragment indicated by an arrow. This is a small light region adjacent to the lower negative spot of the B_z magnetogram. On the magnetogram measured earlier (Figure 8), this fragment is dark and corresponds to the configuration at the time of passage of the active region near the solar disk center (Fig. 6). This fragment retaining its polarity so long can not have changed it for the succeeding 12 hours. This leads us to conclude that from some distance the limb effect tells on the quality of disambiguation (though to a lesser extent) not only in the unsmoothed version of spherical disambiguation. To check the expert assumption about real direction of the field in the said fragment, we conducted one more test: made hand correction of the field direction in this fragment (Figure 9) and extrapolation (Figure 10). A comparison between Figures 6 and 10 shows that the correspondence with the observable loops has not at least gone down.

7. Conclusions

We have presented a new algorithm for removing the 180° azimuth ambiguity. This algorithm is not restricted by the position of magnetograms on the solar disk. Its application to a real near-limb region enabled us to test the FOM method of NLFF limb extrapolation put forward in Rudenko and Myshyakov (2009). The findings of the comparison between the calculated field lines and the real loop structure confirm the effectiveness of the spherical method for removing the azimuth ambiguity and the optimization method FOM for extrapolating nonlinear force-free field the near-limb regions.

Acknowledgements Hinode is a Japanese mission developed and launched by ISAS/JAXA, with NAOJ as a domestic partner and NASA and STFC (UK) as international partners. It is operated by these agencies in cooperation with ESA and NSC (Norway). This work was supported by Grants Nos. 08-02-92204 and 09-02-00226 of the Russian Foundation for Fundamental Research; and Lavrentiev Grant of SB RAS 2010-2011.

References

- Canfield, R. C., de La Beaujardiere, J. F., Fan, Y., Leka, K. D., McClymont, A. N., Metcalf, T., Mickey, D. L., Wulser, J.-P., and Lites, B. W.: 1993, *Astrophys. J.* **411**, 362.
 Cuperman, S., Li, J., and Semel, M.: 1993, *Astron. Astrophys.* **268**, 749.
 Metcalf, T. R.: 1994, *Solar Phys.* **155**, 235.
 Metcalf, T. R., Leka, K. D., Barnes, G., Lites, B. W., Georgoulis, M. K., Pevtsov, A. A., *et al.*: 2006, *Solar Phys.* **237**, 267.
 Metropolis, N., Rosenbluth, A., Rosenbluth, M., Teller, A., and Teller, E.: 1953, *J. Chem. Phys.* **21**, 1087.
 Moon, Y.-J., Wang, H., Spirock, T. J., Goode, P.R., and Park, Y.D.: 2003, *Solar Phys.* **217**, 79.
 Gary, G. A., and D'emoulin, P.: 1995, *Astrophys. J.* **445**, 982.
 Georgoulis, M. K.: 2005, *Astrophys. J.* **629**, L69.
 Georgoulis, M. K., LaBonte, B. J., and Metcalf, T. R.: 2004, *Astrophys. J.* **602**, 446.
 Kirkpatrick, S., Gelatt, C. D., and Vecchi, M. P.: 1983, *Science* **220**, 671.
 Leka, K. D. and Skumanich, A.: 1999, *Solar Phys.* **188**, 3.
 Low, B. C., Lou, Y. Q.: 1990, *Astrophys. J.* **352**, 343.
 Pevtsov, A. A., Canfield, R. C., and Metcalf, T. R.: 1995, *Astrophys. J.* **440**, L109.

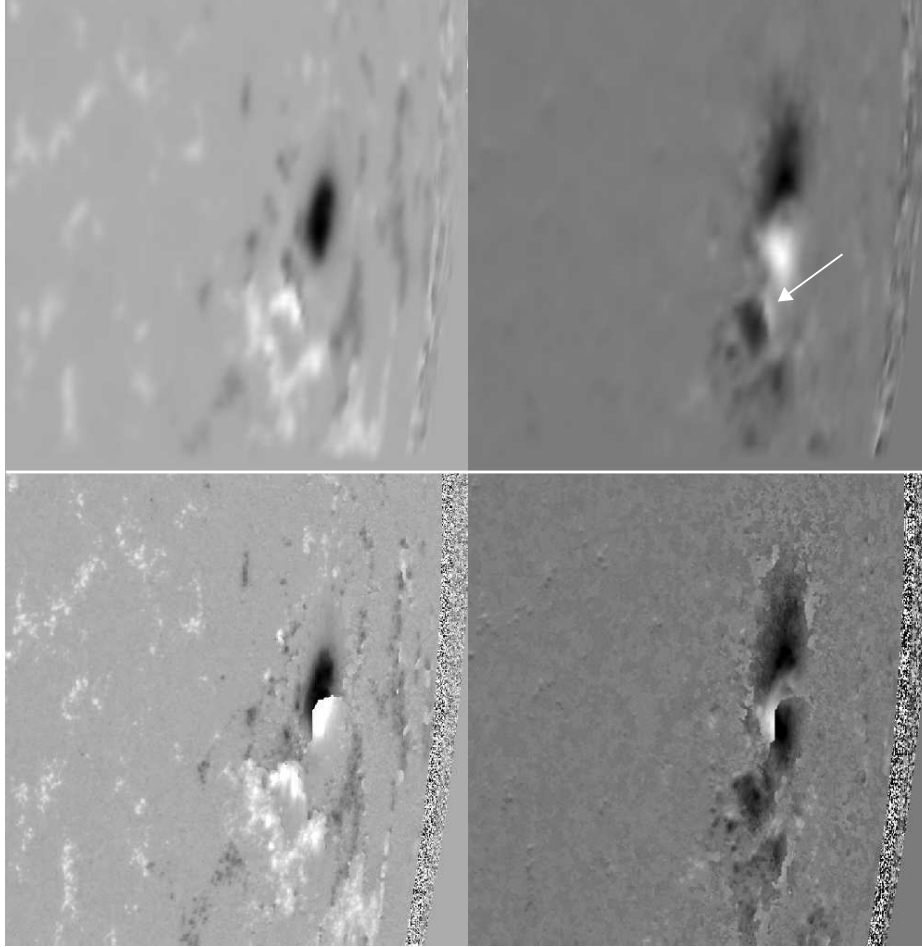


Figure 5. Transverse magnetograms of B_y , B_z : SOT SP (Level2) magnetograms (17 December 2006 0:25:28 UT) after the spherical disambiguation on the quasi-spherical plane with smoothing (top); the same magnetograms after the spherical disambiguation (without smoothing) at high resolution on the grid uniform in the plane of the sky (bottom). The arrow indicates the problem fragment of the top magnetograms

Rudenko, G. V., Myshyakov, I. I.: 2009, *Solar Phys.* **257**, 287.

Schrijver, C. J., Derosa, M. L., Metcalf, T. R., Barnes, G., Lites, B., Tarbell, T., *et al.*: 2008, *Astrophys. J.* **675**, 1637.

Wheatland, M. S., Sturrock, P. A., Roumeliotis, G.: 2000, *Astrophys. J.* **540**, 1150.

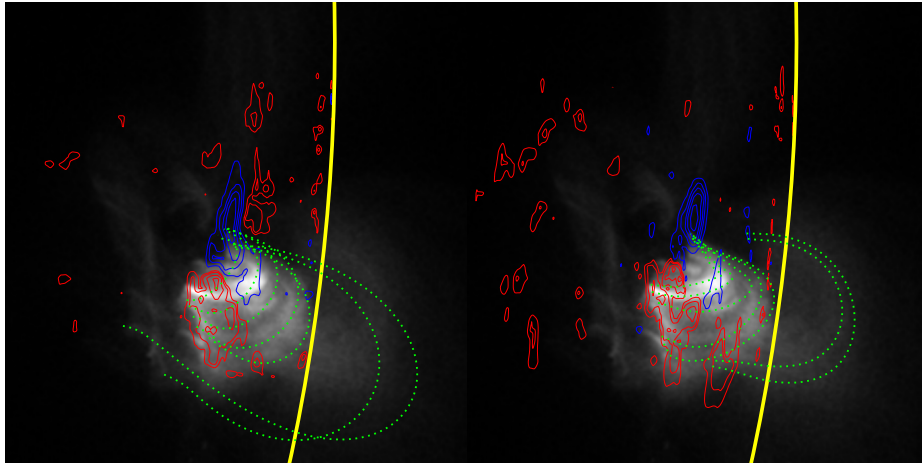


Figure 6. Field lines of the potential (left) and nonlinear force-free (right) fields. At the bottom is the X-ray image from *Hinode* XRT (17 December 2006 0:24:20.5 UT) with changed contrast. Contour lines are distribution of the calculated normal field component; yellow line is the limb

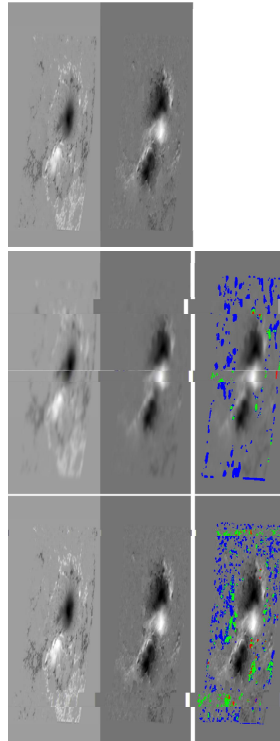


Figure 7. The transverse magnetograms of the model field for 17 December 2006 0:25:28 UT. It was obtained from the magnetogram d of Figure 4: initial model magnetograms (top row); the magnetograms after the spherical disambiguation on the quasi-spherical plane with smoothing (middle row); the magnetograms after the spherical disambiguation (without smoothing) at high resolution on the grid uniform in the plane of the sky (bottom row). To the right of the magnetograms on B_z component are regions of noncoincident directions of the transverse field of the disambiguated and model field magnetograms: blue - $B_t > 1$ Gauss, green - $B_t > 100$ Gauss, red - $B_t > 300$ Gauss; smoothed and unsmoothed magnetograms are compared respectively with smoothed and unsmoothed magnetograms of the model field.

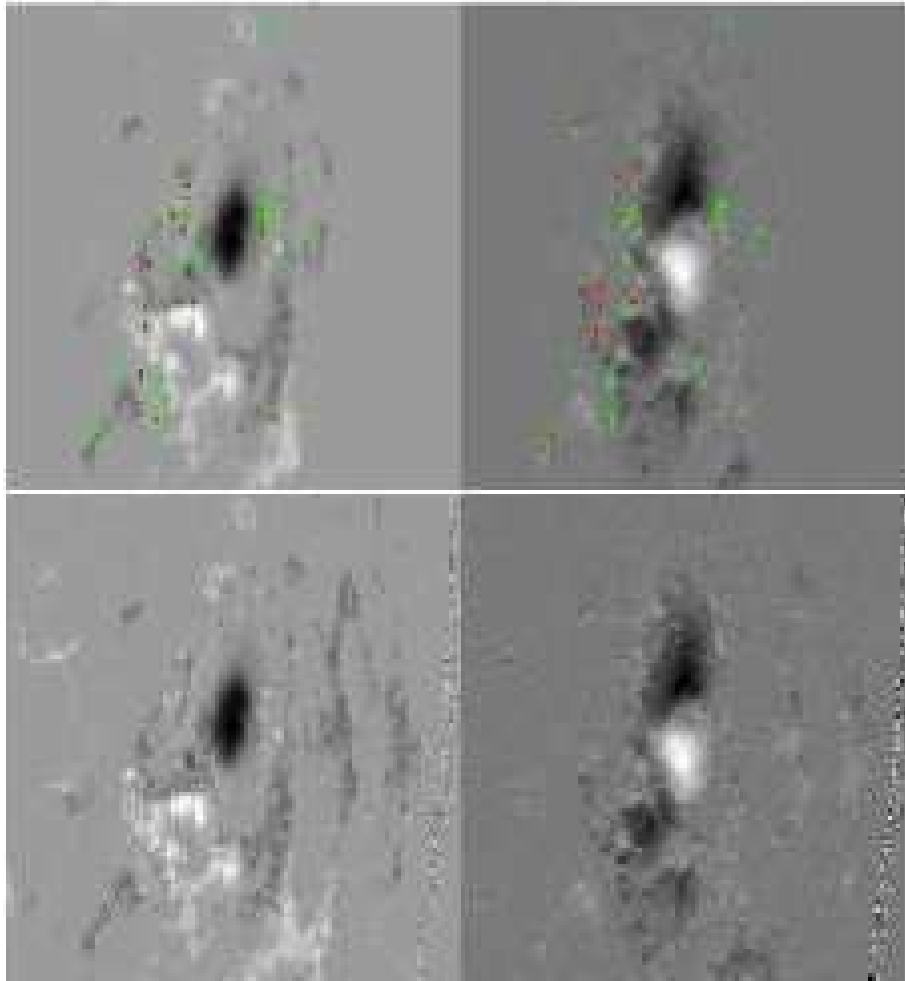


Figure 8. Transverse magnetograms of B_y , B_z : SOT SP (Level2) magnetograms (16 December 2006 12:31:04 UT) after the spherical disambiguation on the quasi-spherical plane with smoothing (top panel); the same magnetograms after the spherical disambiguation (without smoothing) at high resolution on the grid uniform in the plane of the sky (bottom panel). The regions of noncoincident directions of the transverse field on the quasi-spherical plane of the top magnetograms and the bottom magnetogram averaged on the quasi-spherical plane are marked by colors: green - $B_t > 100$ Gauss, red - $B_t > 300$ Gauss.

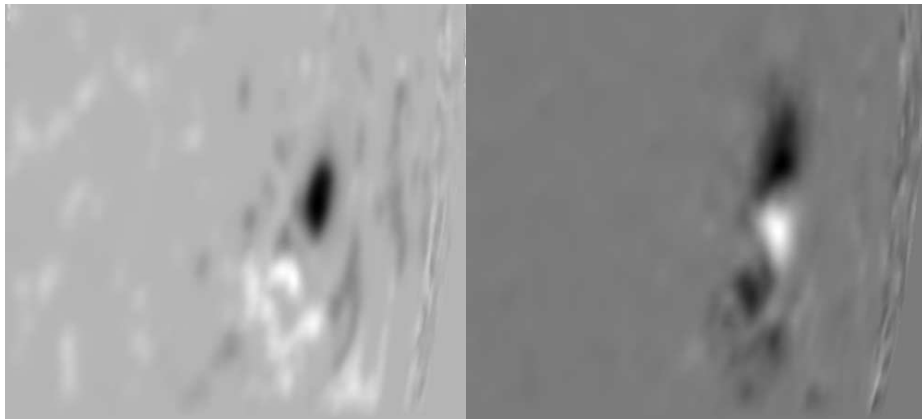


Figure 9. Magnetograms of the upper pair in Figure 5 (17 December 2006 0:25:28 UT) after hand correction of the azimuth direction.

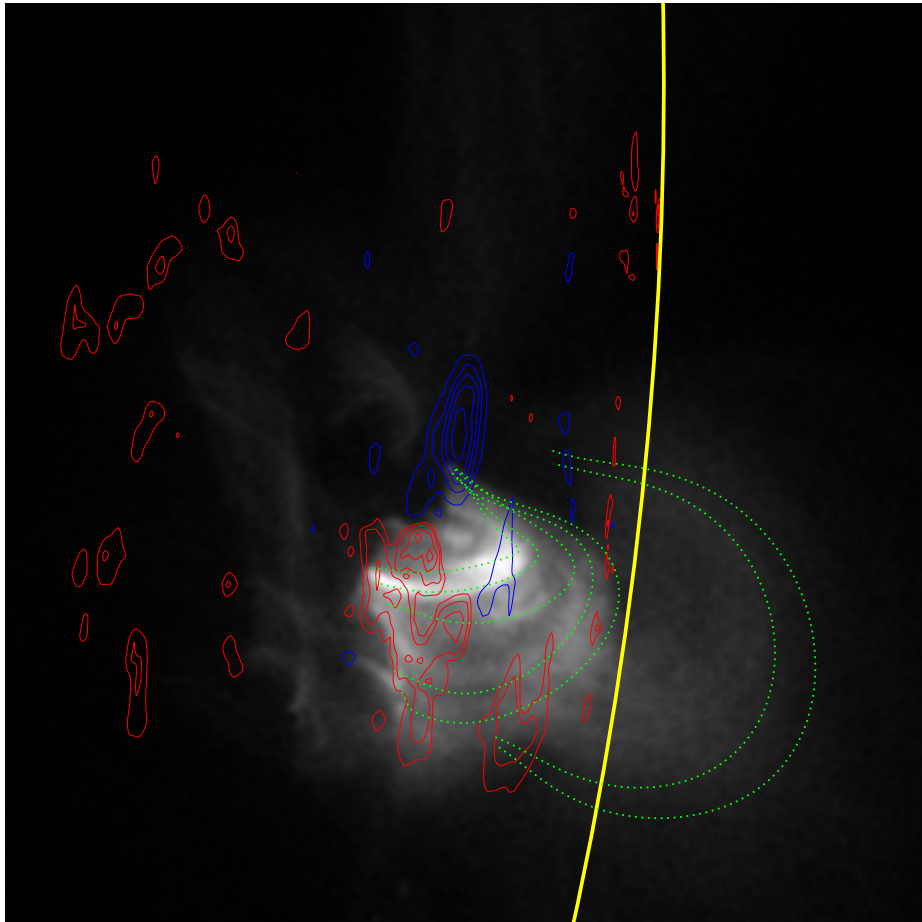


Figure 10. Field lines of the nonlinear force-free field for the boundary field corresponding to the hand-corrected magnetogram in Figure 9. At the bottom is the X-ray image from Hinode XRT (17 December 2006 0:24:20.5 UT) with changed contrast. Contour lines are distribution of the calculated normal field component; the yellow line is the limb.

